# One-dimensional-turbulence simulation of flame extinction and reignition in planar ethylene jet flames

David O. Lignell[a,*], Devin S. Rappleye[a]

[a] *Chemical Engineering Department, 350 CB, Brigham Young University, Provo, UT 84602*

**Abstract**

A series of three simulations of temporally evolving, planar, nonpremixed ethylene jet flames are performed using the one-dimensional-turbulence (ODT) model. The simulations are performed at a fixed Reynolds number, but varying Damköhler numbers, under conditions that result in significant flame extinction and reignition. Results are compared to corresponding direct numerical simulations (DNS), which exhibit 40, 70, and nearly 100% peak flame extinction among the three cases. The planar, temporal configuration is ideal for comparison and validation of the ODT model, and identical thermodynamic, transport, and kinetic models were used. The ODT model captures the jet evolution and heat release effects. Line of sight profiles are qualitatively similar between the ODT and DNS. Good agreement is found for scalar dissipation statistics. While ODT captures the flame extinction process, the level of flame reignition is underpredicted, and conditional mean temperature profiles are depressed during reignition compared to the DNS. This is in contrast to previous ODT studies using $CO/H_2$ mixtures (syngas). As a one-dimensional model, ODT is unable to capture multi-dimensional edge flame propagation during reignition, but is able to capture reignition via flame folding. Given the fidelity of the fine-scale transport and reaction processes built into ODT, and good flow modeling observed, more reduced combustion models will be challenged to capture nonpremixed flame reignition.

*Keywords:* nonpremixed flames, extinction, reignition, one-dimensional-turbulence, simulation

## 1. Introduction

The modeling and simulation of turbulent reacting flows with strong finite rate chemical kinetic effects is a significant challenge. Flows of this type are common in combustion involving pollutant formation (e.g., $NO_x$, and soot), and flame extinction and reignition phenomena. This complexity arises from the wide range of turbulent length and time scales, which cannot be fully resolved in high Reynolds number simulations. Additional complexity arises from the highly nonlinear nature of chemical reaction rates, the presence of complex flame and flow structures, and multicomponent transport effects. In order to develop more advanced and capable combustion models, two important and related types of information are required. First, fundamental information on the physical processes of transport-chemistry interactions in turbulent flows, and second, data for model validation.

Direct numerical simulation (DNS) is an unparalleled tool for probing the details of reacting flows, and is continually improving in its physical realism and range of accessible flows as computational resources expand. Modern DNS, however, require millions of CPU-hours for detailed combustion simulations at low-to-moderate Reynolds number [1]. These simulations are typically computed in isolation, or perhaps including a few parametric extensions to a baseline configuration (variations in Reynolds number, or Damköhler numbers, for instance). This high cost precludes detailed investigation of parameter sensitivity or problem scoping.

The one-dimensional-turbulence (ODT) model is a simulation approach in which high computational costs are mitigated through solution in only a single dimension. Turbulent advection is modeled stochastically by spatial maps (called triplet maps) whose size, location, and frequency are implemented in a manner consistent with turbulent scaling laws, based on the local instantaneous velocity field. These maps increase scalar gradients and isosurface area in a manner consistent with corresponding turbulent advection. In ODT, velocity components, and optionally scalars such as energy and chemical species, are solved via unsteady one-dimensional transport equations in the line direction. Triplet maps are implemented concurrently with these diffusive-reactive processes. Hence, the ODT model may provide useful information for model validation and parametric investigation of turbulent flows at a cost orders of magnitude lower than that of DNS. While it is not implied that ODT is a replacement for DNS, there is a relatively large gap between DNS with full resolution and large eddy simulation (LES), which requires modeling of all fine, unresolved flow and chemical structures. In this sense, ODT may play an important intermediate role, by

*Corresponding Author; Tel.: (801) 422-1772; Fax: (801) 422-0151; Email: davidlignell@byu.edu

resolving structures in one dimension, with stochastically-modeled turbulent motions the compromise for computational efficiency.

Since Kerstein developed the ODT model in 1999 [2], the model has undergone continual improvement and application to a wide range of flow phenomena. Kerstein et al. [3] presented a vector formulation of the model in which all three velocity components are retained to model pressure-scrambling and associated return-to-isotropy effects. Ashurst and Kerstein [4] developed a variable density formulation of the model and also introduced a spatial formulation of the model in which evolution along the line occurs in a spatial (rather than temporal) coordinate by invoking standard boundary layer assumptions. This variable density formulation is crucial for combustion simulation. The model has been successfully applied to non-reacting flows including homogeneous turbulence [2], wakes [5], wall-bounded buoyant flows [6, 7], mixing layers [2, 3, 4, 8], Rayleigh-Benard convection [9], and layer formation in stably stratified turbulent flows [10]. In addition to its use as a standalone model for solving various flow configurations, the model has been applied in conjunction with the LES model in channel flows [11], as a near-wall LES closure [12], and as an LES subgrid closure model [13, 14, 15]. The variable density formulation of the model has enabled application to studies of turbulent combustion. Echekki et al. [16] applied the ODT model to turbulent jet diffusion flames. Ranganath and Echekki used ODT as a subgrid tabulation-based model used with RANS of a hydrogen jet flame [17] and also in a piloted methane jet flame with flame extinction [18]. Shihn and DesJardin [19] studied near-wall behavior for vertical wall fires with acetylene and propane fuels. Hewson and Kerstein used the model directly to study syngas flames [20], including a detailed study of flame extinction and reignition in these flames [21]. Ricks et al. used the ODT model to study soot and enthalpy evolution in buoyant fires [22]. Hewson et al. [23, 24] developed and validated a new conditional moment closure (CMC) model for soot formation using the detailed information that ODT provides to evaluate unclosed terms in the CMC equations along with the modeled closures. The study was subsequently validated using DNS data [25], highlighting the use of ODT as a DNS surrogate.

In this paper, we present a direct comparison between ODT and DNS for temporally evolving ethylene jet flames with extinction and reignition phenomena. While previous ODT studies have considered flames with these phenomena, comparison to DNS data allows a more consistent and direct comparison, with more detailed statistical information provided, equivalent chemistry and transport models, and consistent flow configurations. The DNS simulations have been described in detail in [26]. The planar, temporally evolving jet consists of periodic flow in an axial direction, with two directions of statistical homogeneity, and a single shear direction. This configuration, elaborated on below, is ideal for temporal ODT. A previous comparison of ODT to DNS data was performed by Punati et al. [27]. Those simulations were compared to the medium Reynolds number case of a series of three temporally evolving $CO/H_2$ jet flames with varying Reynolds number under conditions of extinction and reignition [28]. Punati et al. found good qualitative agreement between the ODT and DNS. Flame extinction was followed by strong reignition so that conditional temperatures at the end of the simulation were very similar between the ODT and DNS. The ODT extinction occurred somewhat prior to that of the DNS and was more intense, while the ODT reignition was also stronger. These results are in contrast to those of the present simulations (discussed further below).

The present simulations include a comparison to three DNS cases at constant Reynolds number, but varying Damköhler number. The three parametric studies are a novel feature of the present work and illustrate the ability of ODT to capture a range of flames. This paper further contributes to the understanding of the capabilities of ODT as a standalone model for flame extinction and reignition by expanding the range of fuels studied, and by providing sensitivities to model parameters. The ethylene fuel employed here exhibits a high degree of flame extinction, with evidence for reignition through premixed flame mechanisms [26]. Additionally, ethylene is a complex fuel with a high activation energy and narrower reaction zone relative to syngas (used by Punati et al. [27] and Hewson and Kerstein [20, 21]).

Flame extinction and reignition phenomena are important processes in combustion that are notoriously difficult to model accurately. Our goals are to present validation results of the model including the jet evolution, mean and fluctuating quantities in physical and mixture fraction coordinates, and quantify limitations of the model. Our hope is that ODT will provide sufficient agreement with DNS to be useful in developing and validating combustion models, and for further use in conjunction with hybrid LES approaches.

## 2. Numerical implementation

The following sections describe the ODT code used in this study along with a description of the DNS cases being compared.

### *2.1. ODT description*

ODT is described in detail in the literature presented above. A summary of the approach is presented here, along with a description of the model implementation.

#### *2.1.1. Advection processes (eddy events)*

ODT evolves the unsteady momentum, energy, and species transport equations in one dimension. Advection processes representing turbulent transport are implemented as discrete eddy events involving triplet maps that rearrange fluid on the domain. These triplet maps occur concurrently with the diffusion processes. The triplet maps

are parameterized by a size $l$, position $x_o$, and time scale $\tau$. The triplet map is implemented by taking all property profiles in the eddy region, making three copies, compressing each spatially by a factor of three, and replacing the original profiles by the three compressed copies with the middle copy inverted spatially. This process is illustrated schematically in Fig. 1. The figure shows a DNS of a single vortex (eddy) in a Kelvin Helmoholtz instability (a key process in shear-driven turbulence), along with the mixture fraction profile before and after the eddy, and a schematic of the triplet map. The triplet map is conservative of all quantities, is continuous, and has the desired properties of increasing scalar gradients and decreasing length scales, as occur in turbulent processes. In the present ODT code, a finite volume method is used with adaptive cell sizes (discussed further below). The triplet map is implemented analytically assuming piecewise constant property profiles in cells. The cells are split where eddy edges intersect the cell. During the triplet map, cells are compressed by a factor of three and the center cells of the map are spatially inverted. This is in contrast to ODT formulations using a discrete permutation of cells that requires a transport correction [29] and limits eddy sizes to integer multiples of three of the grid spacing.

The ODT velocity profile evolves through the specification of the occurrences of eddy events. Conversely, the velocity profile supplies information that determines the size, location, and frequency of these events. The eddy selection process is stochastic and follows the variable density formulation of Ashurst and Kerstein [4]. The eddy time scale $\tau$ for a candidate eddy of position and size $(y_0,\, l)$ is computed using a measure $E_{\text{kin}}$ of the local kinetic energy in the eddy region (see Eq. 3 below) and the scaling: $E_{\text{kin}} = \frac{1}{2}\rho_0 l^3/\tau^2$, where $\rho_0$ is a measure of density on the eddy region (see Eq. 3). The local rate (per square length) of eddy $(y_0,\, l)$ is taken to be $\lambda = 1/l^2\tau$, and the total rate of all eddies is $\Lambda = \iint \lambda dy_0 dl$. Hence, the joint PDF of eddy parameters $y_0$ and $l$ is $P(y_0,\, l) = \lambda(y_0,\, l)/\Lambda$. Eddy occurrences can be sampled from a Poisson distribution with mean rate $\Lambda$, with $y_0$ and $l$ parameters sampled from $P(y_0,\, l)$. $P(y_0,\, l)$ can be evaluated, but in practice this is prohibitively expensive since it changes continuously as the velocity profile changes. In effect, the time scales of all possible eddies would need to be computed to obtain $P(y_0,\, l)$, which would then be used to sample the next eddy. But after a single eddy were implemented (and associated diffusive advancement occurs), $P(y_0,\, l)$ would need to be recomputed. Instead, a thinning process [30] based on the rejection method [31] is used. Eddies are sampled from an analytic approximation to $P(y_0, l)$, denoted $\tilde{P}(y_0, l)$, and accepted with probability

$$P_a = \Delta t_s/(\tau \tilde{P}(y_0,\, l) \cdot l^2). \tag{1}$$

$\tilde{P}(y_0,\, l)$ is modeled as $\tilde{P}(y_0,\, l) = f(l) \cdot g(y_0)$. The PDF $g(y_0)$ is uniform on the domain $y_0 \leq 0 \leq L_y - l$ ($L_y$ is the domain length), and $f(l)$ is given by S. Wunsch (described in [29]):

$$f(l) = \frac{-2l_p}{l^2}\left(\frac{\exp(-2l_p/l)}{\exp(-2l_p/l_{max}) - \exp(-2l_p/l_{min})}\right), \tag{2}$$

where $l_p$, $l_{max}$, and $l_{min}$ are user-specified most probable, maximum, and minimum eddy sizes, respectively. Values used in the simulations are $l_p/L_y = 0.05$, $l_{max}/L_y = 1$, and $l_{min}/L_y = 0.004$. The function $f(l)$ reasonably approximates the shape of the eddy PDF. The accuracy of $f(l)$ only affects the eddy sampling efficiency, which is not the limiting step in the ODT simulations (the diffusive-reactive advancement is).

In Eq. (1), the time $\Delta t_s$ between eddy trials is sampled from a Poisson distribution with mean $\overline{\Delta t_s}$. This mean sample time is initialized as $\overline{\Delta t_s} = 0.1\overline{P_a} \cdot \overline{\Delta y}^2/\nu n$, where $\nu$ is kinematic viscosity, $n$ is the number of grid points, $\overline{\Delta y}$ is the average grid size, and $\overline{P_a}$ is a specified average acceptance probability (set to 0.02). $\overline{\Delta y}^2/\nu$ is a diffusive time at the grid cell size, (an approximate lower bound on an eddy timescale). The factor $1/n$ allows sampling of this small diffusive scale eddy in all cells (on average). The 0.1 multiplier is a conservative factor. $\overline{\Delta t_s}$ is dynamically adjusted during the simulation to maintain the specified $\overline{P_a}$.

The eddy time scale $\tau$ is computed as

$$\frac{1}{\tau} = C\sqrt{\frac{2}{\rho_0 l^3}(E_{\text{kin}} - ZE_{\text{vp}})}, \tag{3}$$

where $E_{\text{kin}}$ is a measure of kinetic energy as in [4, 32], and $\rho_0 = l^{-3}\int \rho K(y)^2 dy$, where $K(y)$ is the kernel function used in the vector formulation of ODT [3, 4]. $E_{\text{vp}}$ is a viscous penalty defined using scaling arguments as $E_{\text{vp}} = \frac{1}{2}\bar{\mu}^2/\bar{\rho}l$, where $\bar{\rho}$ and $\bar{\mu}$ are the average density and viscosity in the eddy region. The parameters $C$ and $Z$ are adjustable model parameters.

For open domains, a restriction must be imposed on the eddy selection process to avoid unphysically large eddy events from occurring. This is termed large eddy suppression and several methods have been employed including the median and scale reduction methods [4], and the elapsed time method [16, 20]. Here, the elapsed time method is used. The criterion

$$t > \beta\tau \tag{4}$$

is applied so that eddies are only allowed if the elapsed time is greater than $\beta\tau$, where $\beta$ is an adjustable parameter.

*2.1.2. Diffusive advancement*

The diffusive advancement of the simulation occurs concurrently with eddy events. An adaptive-grid, object-oriented ODT code was developed for this investigation. The code is written in C++ and parallelized with MPI to facilitate simulation of multiple realizations. The adaptive grid allows grid cells to be split and merged, and cell faces to float [33].

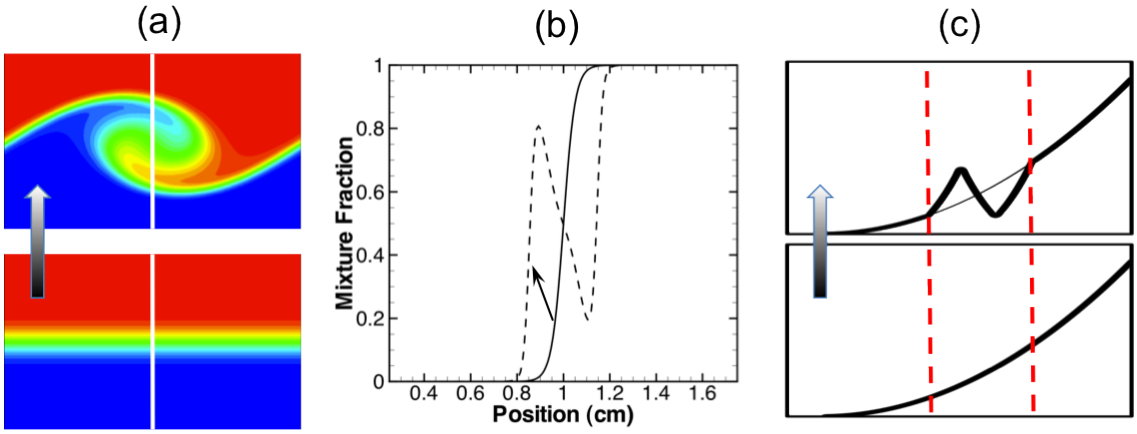


Figure 1: Illustration of the triplet map. (a) mixture fraction field in a Kelvin-Helmholtz instability before and after an eddy; (b) the corresponding profile through the indicated line of sight; (c) a schematic illustration of the triplet map in ODT.

The diffusive advancement is implemented using a Lagrangian finite volume method in which cell faces move with the mass average velocity. This velocity is distinct from the three velocity components evolved in ODT, which exist solely to specify the advective eddy events consisting of triplet maps followed by velocity modifications modeling pressure scrambling. Cells expand and contract due to flow dilatation arising from heat release and heat and mass transfer processes. During diffusive advancement, the total mass in a given grid cell is constant, and the continuity equation reduces to

$$\rho \Delta y = \text{constant}. \tag{5}$$

In all equations, $y$ is the line direction.

The transport equation for reactive species is given by

$$\frac{dY_i}{dt} = -\frac{1}{\rho \Delta y}(j_{i,e} - j_{i,w}) + \frac{\omega_i}{\rho}, \tag{6}$$

where $\omega_i$ is the species reaction rate, and $j_{i,e}$, $j_{i,w}$ are the species diffusion fluxes on the east and west cell faces, respectively. The constitutive relation for the diffusion flux is identical to that used in the DNS:

$$j_i = -\frac{\rho Y_i D_i}{X_i}\frac{dX_i}{dy} = -\rho D_i \frac{dY_i}{dy} - \frac{\rho D_i Y_i}{M}\frac{dM}{dy}, \tag{7}$$

where $M$ is the mean molecular weight, and $D_i$ and $X_i$ are the species diffusion coefficient and the mole fraction of species $i$, respectively.

The momentum transport equations are given by

$$\frac{du_k}{dt} = -\frac{1}{\rho \Delta y}(\tau_{k,e} - \tau_{k,w}), \tag{8}$$

where $u_k$ is one of $u$, $v$, and $w$, and $\tau_k$ is the component viscous stress modeled as

$$\tau_k = -\mu \frac{du_k}{dy}. \tag{9}$$

The energy equation is given simply by

$$\frac{dh}{dt} = -\frac{1}{\rho \Delta y}(q_e - q_w) \tag{10}$$

The heat flux $q$ includes thermal conduction and species mass flux terms:

$$q = -\lambda \frac{dT}{dy} + \sum_i h_i j_i. \tag{11}$$

The enthalpy is related to the temperature and species through the auxiliary relation $h = h(T, Y_i)$ using composition and temperature dependent heat capacities and assuming ideal gases.

These equations differ from those solved in the DNS by the implied low Mach assumption, the neglect of kinetic energy and viscous heating in the energy equation, and the approximate form of the viscous stress (along with the one-dimensional treatment of advection and diffusion). All thermophysical and transport properties are computed using the Cantera software package [34]. The chemical mechanism used is the same as in the DNS. The mechanism is a reduced ethylene mechanism consisting of 19 transported species, 10 quasi-steady species, and 167 chemical reactions [35].

The numerical solution of the diffusive transport equations assumes uniform scalar profiles in grid cells, and applies central differences at control volume faces. A first-order (Euler) semi-implicit integration is performed in time for simulations presented. A second-order (modified midpoint [36]) method is also implemented. No significant differences were found in the results using the second-order method. The method is semi-implicit in that chemical reactions are integrated implicitly using CVODE [37], but diffusion is performed explicitly. This implicit integration is performed to compute a mean reaction rate for use in the otherwise explicit solver. In explicit Runge-Kutta methods ($y' = f(y)$), all stages are computed assuming constant values for the rate $f(y)$ during the given stage.

In the method developed here, the species and enthalpy equations (given above) are integrated over the stage using CVODE, but the diffusive terms in those equations are assumed constant. (Enthalpy is not included in the CVODE solution array since its value varies linearly with the assumed constant rate arising only from the heat flux). The mean chemical reaction rate over the stage is then computed as

$$\left\langle \frac{\omega_i}{\rho} \right\rangle = \frac{Y_i^* - Y_i}{\delta t} + \left( \frac{1}{\rho \Delta y} (j_{i,e} - j_{i,w}) \right), \qquad (12)$$

where $Y_i^*$ is the result of the implicit CVODE integration. This mean rate is then used in place of the reaction source term in the species equation in the explicit integration. This method results in an accurate and stable method which advances at a diffusive CFL and overcomes stiff chemistry limitations. The reaction and diffusion processes are more tightly coupled in this method than in standard splitting approaches.

The diffusion implementation was verified by comparison with a one-dimensional DNS (a relaxing nonpremixed ethylene flame) under identical initial conditions with excellent agreement.

*2.1.3. Mesh management*

The computational mesh is dynamically adapted throughout the ODT simulation. In particular, triplet maps increase the number of grid points in the eddy region by a factor of three. Dilatation during the diffusion process also alters the grid. The mesh is adapted by specifying controlling profiles (such as streamwise velocity and temperature). These profiles are normalized to vary on [0,1] on both the domain and range. For a single profile, grid points are chosen so that they are spaced equally along the curve of the normalized profile. This is done by defining a distance function as simply $s_i = \sqrt{\delta f_i^2 + \delta y_i^2}$ for normalized profile $f(y)$. The cumulative distance is computed and divided into equal increments (giving a new distance function) using a grid density parameter (points per unit length along the curve), and new mesh points are computed by interpolation between the old and new distance functions. Simultaneous adaption of multiple profiles is treated simply by taking $s_i$ at a given point as the largest for all considered profiles at that point. This may result in a region where one profile is flat and another is varying being over-resolved in the flat profile (see Fig. 2).

The revised grid is then processed to eliminate cells smaller than a specified minimum (less than 20 $\mu$m for the cases considered here). Offending grid cells are processed in order of increasing size, and each offender is merged with its smaller neighbor until it is larger than the minimum. The grid is then processed so that adjacent cell size ratios (larger divided by smaller) are no larger than a factor of 2.5. Offending cells are split by factors of two until this bound is satisfied. The original ODT line is then mapped to the revised grid by splitting cells to create faces that occur only in the new grid, then by merging cells to eliminate faces that occur only in the old grid. The merging and splitting conserves time advanced properties, but not their higher moments, under the assumed uniform cell profiles. Cell splitting is done with a conservative, parabolic interpolant for cells that are not critical points. A given cell may be split into several cells at once (e.g., by the 2.5 rule). Figure 2 shows the initial adapted temperature and velocity profiles for Case 1 with these variables as the adaption variables. Note the high resolution in the flat region of the velocity profile due to the resolution of the temperature profile.

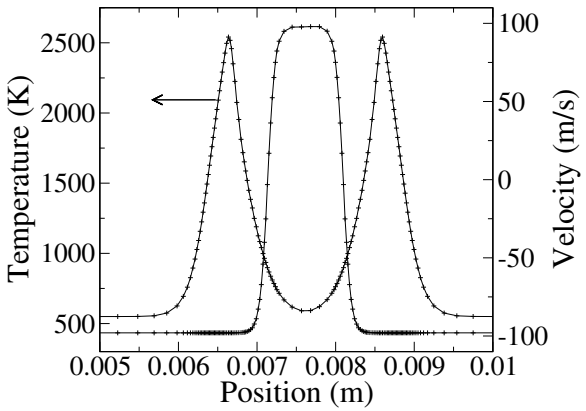


Figure 2: Initial temperature and velocity profiles for Case 1 illustrating adapted mesh profiles.

*2.2. Configurations of the DNS and ODT cases*

The DNS cases are described in detail in [26], and only a brief summary of the cases is provided here. The configuration is a temporally evolving, planar ethylene jet flame at a nominally constant pressure of 1 atm. A central planar slab of fuel is surrounded by oxidizer. The main flow direction (streamwise) is in the x-direction, which is periodic. The z-direction (spanwise) is also periodic and the fuel slab is in the x-z plane. Outflow boundary conditions are applied in the y-direction (cross-stream), which is the direction of mean shear. The DNS are spatially homogeneous in the streamwise and spanwise directions, with mean variations occurring in the cross-stream direction.

The ODT lines in the present simulations are oriented in the cross-stream direction. A single ODT line simulation is performed as a single realization of the corresponding DNS case. Statistics, such as means and fluctuations, are gathered from an ensemble of ODT realizations that differ only in the choice of random number seed.

The DNS is initialized with a smoothed top-hat velocity profile of width $H$ in the streamwise direction. A tanh transition between the fuel and oxidizer stream velocities (of difference $\Delta U$) of transition width $\delta_u$ is used. Velocity fluctuations consistent with an isotropic homogeneous turbulence spectrum are overlaid in the fuel core region to trip the mean velocity shear layers (with fluctuation $u'$, and $L_{11}$ specified). The flame is initialized with a

Table 1: Simulation parameters of the three parametric DNS cases. Repeated values (e.g., on $L_y$) refer to values for DNS Cases 1, 2, and 3, respectively [26].

| | | | |
|---|---|---|---|
| H (mm) | 0.96 | $L_x/H$ | 12 |
| $\Delta U$ (m/s) | 196 | $L_y/H$ | 15, 17, 19 |
| $Re_{jet}$ | 5120 | $L_z/H$ | 8 |
| $H_\xi$ (mm) | 1.5 | $\Delta y$ ($\mu m$) | 17 |
| $\delta_u$ (mm) | 0.19 | $\delta_\xi$ (mm) | 0.74 |
| $u'/\Delta U$ (init) | 5% | $\tau_{jet}$ (ms) | 0.0049 |
| $H/L_{11}$ (init) | 3 | $\tau_{run}/\tau_{jet}$ | 74, 87, 140 |

Table 2: Stream compositions (mole fractions) for the three cases [26].

| | | Case 1 | Case 2 | Case 3 |
|---|---|---|---|---|
| $\xi = 0$ | $O_2$ | 0.33516 | 0.30525 | 0.26914 |
| | $N_2$ | 0.66484 | 0.69475 | 0.73086 |
| $\xi = 1$ | $C_2H_4$ | 0.52105 | 0.47642 | 0.47205 |
| | $N_2$ | 0.47895 | 0.52358 | 0.57795 |

smoothed top-hat profile of width $H_\xi$ and transition width $\delta_\xi$. A steady laminar flamelet solution at $\chi = 0.5\chi_{\text{quench}}$ is mapped to the mixture fraction profile. Table 1 shows the configuration parameters, where $L$ is the domain size, $\tau_{jet} = L_x/\Delta U$, and $\Delta y$ is the grid spacing.

The DNS are performed at the same Reynolds number, but varying Damköhler number. This is achieved by varying the fuel and oxidizer stream compositions, resulting in Cases 1, 2, and 3 having increasing levels of flame extinction. Table 2 shows the stream compositions for the three cases.

The ODT simulations are initialized using the cross-stream DNS profiles for temperature and composition, and the (x-z) planar mean DNS profiles for the three velocity components.

## 3. Results

ODT simulations are performed for each of the three levels of flame extinction represented in the DNS, and referred to as Case 1, Case 2, and Case 3, respectively. Baseline simulations are performed for all cases with a single set of values of ODT parameters consisting of $C$, $Z$, and $\beta$, of which only $C$ and $\beta$ are tuned to match DNS results (primarily jet evolution and scalar dissipation rate). $C$ and $\beta$ sensitivities of some of the results are also mentioned. Wide variations in $C$ and $\beta$ were studied with $C$ from 0.1 to 30, and $\beta$ from 0.4 to 1.0. Baseline values chosen for all three cases are $C = 8$, $\beta = 0.8$, $Z = 400$ based on the evolution of the mixture fraction, the conditional temperature profiles, and the scalar dissipation rate, discussed below.

For each case, 512 realizations are conducted, which is sufficient to yield adequately converged statistics. Figure 3 shows the centerline mixture fraction at 0.36 ms for Case 1 (here $C = 3$, $\beta = 0.6$). The figure shows the convergence versus the number of realizations. The upper curve is the average centerline value using the corresponding number of realizations. The lower plot is the error as measured by

$$\text{Error} = \left| \frac{1}{n} \sum_{i=1}^{n} \xi_i - \frac{1}{1024} \sum_{i=1}^{1024} \xi_i \right| . \qquad (13)$$

This error decays as $\sqrt{n}$ (dashed line), in accordance with the central limit theorem. The fluctuations (error) after 512 realizations are below 1%. The cost per realization is approximately 15 min on 2.8 GHz Intel Nehalem processors. Simulations were performed in parallel with each realization assigned to a given processor (128 realizations in a batch).

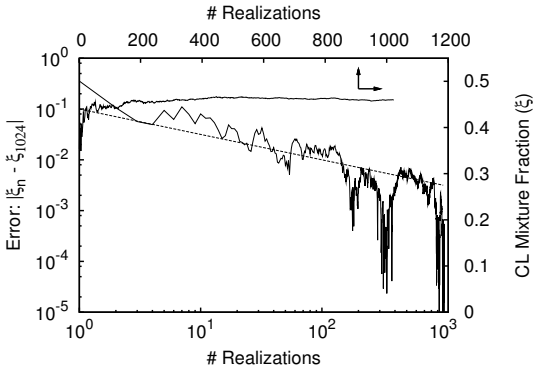


Figure 3: Centerline mixture fraction versus number of realizations for Case 1 at 0.36 ms. The top curve shows the mean value using the number of realizations. The lower curve shows the difference between the mean at a given number of realizations and after 1024 realizations. The dashed line has slope consistent with a $\sqrt{n}$ convergence.

Figure 4 shows instantaneous profiles of temperature and mixture fraction for Case 1 at t=0.15 ms. The ODT profile represents one of the 512 realizations, while the DNS represents a line at an arbitrary x, z location. Naturally, one realization differs markedly from another so the comparison is qualitative. However, the profiles shown are qualitatively very similar and show the fluctuations induced by the ODT eddy events. The resulting diffusive processes will differ primarily in the restriction of ODT to one-dimensional structures. However, the resolution of the primary strain direction, with physically realistic strain profiles, is an advantage of ODT. For these studies, the grid density parameter for mesh adaption was set at 30, with a smallest cell size approximately that used in the DNS (17 $\mu$m). Case 1 was also run with twice the grid density, and a smallest cell size less than half that of the DNS, with no significant differences in the jet evolution, temperature, OH mass fraction, or scalar dissipation profiles.

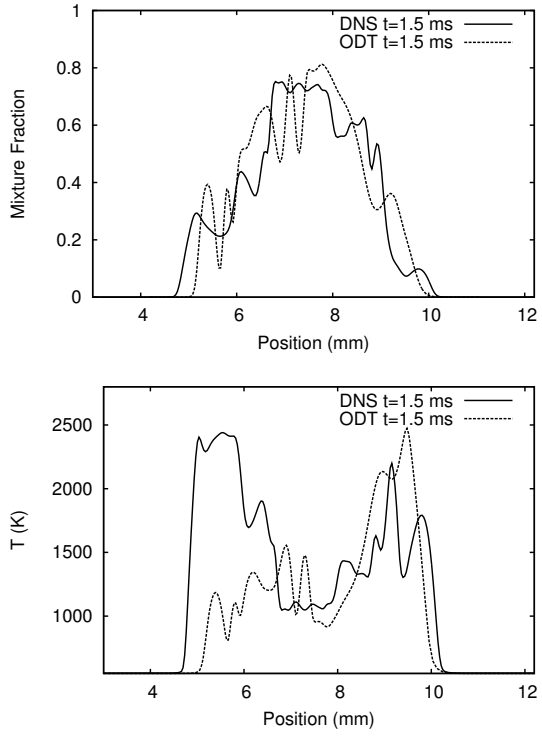


Figure 4: Instantaneous mixture fraction and temperature profiles for ODT and DNS for Case 1 at 0.15 ms.

### *3.1. Jet evolution*

The jet evolution is presented in Fig. 5, which shows the mean and root mean square (RMS) fluctuations of mixture fraction along the axial centerline (cL) as a function of time. Also shown is the width of the profile measured at half the maximum (centerline) value (FWHM). Figure 6 shows the full evolution of the mean mixture fraction profile for Case 2.

The FWHM mixture fraction increases with time, while the centerline value decreases. The ODT and DNS results are shown for each case. Good qualitative agreement, and fair quantitative agreement, is observed for the three cases. The level of flame extinction in the DNS is extreme, at 40%, 70% and nearly 100% for Cases 1, 2, and 3, respectively, as measured by the fraction of the stoichiometric surface with an OH mass fraction below half the steady laminar extinction value. The high degree of extinction impacts the jet evolution. The DNS FWHM profile for Case 3 increases sharply, then levels off around 0.2 ms, then rises sharply again at 0.4 ms. These times correspond with the times of major extinction of the flame, and the reignition process, which results in flow dilatation through heat release. This behavior is also observed in Case 2 but to a somewhat lesser extent. The ODT profiles for all three cases show a fairly steady rise in the width. There is a trend of decreasing FWHM with increasing case number (extinction level) for the ODT compared to the DNS, while the centerline value is increasing relative to the DNS.

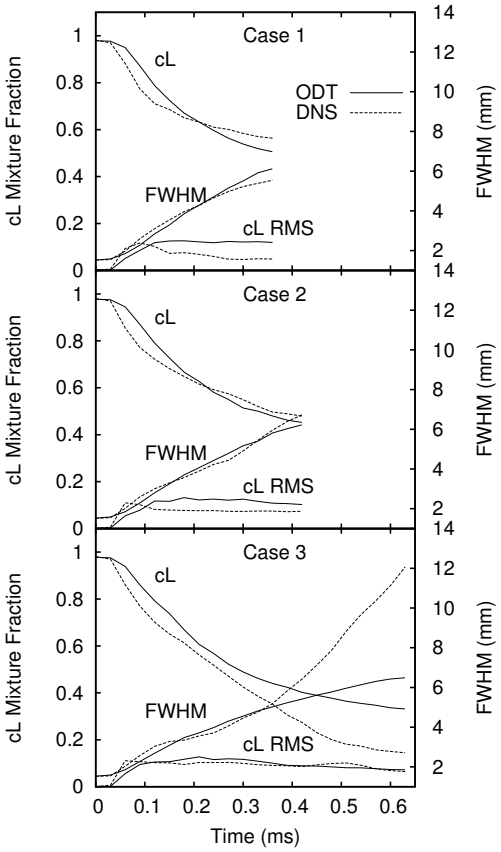


Figure 5: Centerline and full width at half maximum values of mean and RMS fluctuations of mixture fraction.

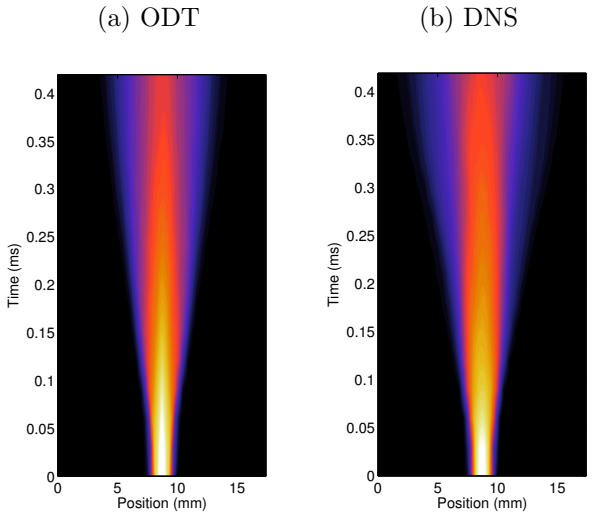


Figure 6: Mean mixture fraction profiles for Case 2.

The agreement with the DNS for Case 3 is poor at later times. These properties are largely due to the degree of reignition, discussed further below.

These simulations have an advantage over previous ODT comparisons to experiments (e.g., [16, 20]) in that difficulties associated with comparing planar, temporally evolving ODT to cylindrical, planar jet flames are removed. The flames expand only in the cross-stream direction (in the mean) for the present configuration.

### *3.2. Extinction and reignition*

The degree of flame extinction and reignition that is captured by the ODT model is of primary importance. These processes are presented in terms of mean and RMS profiles conditioned on the mixture fraction.

Figure 7 presents the conditional (on mixture fraction) mean temperature profiles as a function of the mixture fraction for several times. The top row is the ODT, and the bottom row is the DNS. In each case the stoichiometric mixture fraction is $\xi = 0.17$. Five or six times are chosen that include the initial and final times, times close to the peak flame extinction (which occurs at 0.14, 0.18, and 0.38 ms, for Cases 1, 2, and 3, respectively), and intermediate times. In the figure, thin lines represent times of extinction-dominated processes, and thick lines, at the two or three final times shown, represent the times of reignition-dominated processes. The vertical lines at the right of each plot indicate the upper bound of the mixture fraction range in the domain at the given time to show the progression of the peak mixture fraction. 60 bins are used in the mixture fraction coordinate for conditional statistics. Figure 7 is augmented by Fig. 8, which shows the stoichiometric mean temperature versus time for each ODT and DNS case on the same plot for direct comparison.

Each case starts with a burning solution. There is a short initial transient during which the flat flames relax as the turbulence begins to develop. The flames then become strained and begin to extinguish as the turbulence develops from the mean shear instabilities. The temperature drops during flame extinction and reaches a minimum at the point of peak flame extinction. Local flame strain then decreases as the large and small scales increase as the jet evolves, allowing the flame to reignite. This process is also highlighted in Fig. 8, which shows the stoichiometric mean temperature for each case as a function of time. Both the DNS and the ODT show a trend of decreasing, then increasing conditional mean temperature. Additionally, the ODT reproduces the increasing level of extinction with increasing case number (decreasing Damköhler number). The ODT minimum temperatures are 200-300 K lower than the DNS for Cases 1 and 2. These two cases show higher levels of flame extinction than the corresponding DNS, while Case 3 does not achieve the same level of flame extinction as the DNS. In interpreting these results it is important to note that the DNS for Case 3 show nearly 100% flame extinction, with only a single burning kernel that survives to reignite the flame. Hence, it is unlikely that the ODT will achieve the same level of flame extinction without extinguishing globally.

While ODT does exhibit flame reignition as evidenced by the rise in the conditional mean temperature profiles, the degree of reignition is underpredicted. This underprediction increases with increasing case number. For Cases 1 and 2, the ODT temperature attains approximately half the difference between the minimum and maximum mean temperatures, while the Case 3 temperature recovery is significantly less. The temperature recovery for the ODT and DNS is nearly the same for Case 1 (see Fig. 8), but the ODT for that case has higher extinction and hence less reignition. Cases 1 and 2 of the DNS achieve nearly complete reignition, with the conditional temperature profiles at the end of the simulation closely matching those at the beginning of the simulation. In Case 3, the DNS do not achieve a complete relight of the flames due to insufficient simulation time. (The domain would not support the flame size were the case run longer.) However, the conditional profiles exhibit a very strong and noticeable rise in temperature around the stoichiometric point. Case 3 of the ODT achieves both a lower degree of flame extinction, and a lower degree of flame reignition.

As the jet evolves, the peak mixture fraction attained in the domain decreases, as is evident in the upper mixture fractions for the conditional mean temperature profiles (see Fig. 7). The peak mixture fractions are higher in the ODT than in the DNS, consistent with the results of Fig. 5.

Figure 9 shows the conditional RMS fluctuations of temperature about the mean. While the conditional means of the ODT exhibited the same trend as the DNS, the conditional RMS do not. For the ODT, the conditional RMS show a consistent and sustained rise in the vicinity of the flame. Conversely, the conditional RMS for the DNS both rise and fall. For Cases 1 and 2 of the DNS, the conditional RMS begins low, then rises through the extinction and reignition processes where there are many regions of the same mixture fraction with states intermediate between burning and quenched. Finally, as the flames approach complete relight, the fluctuations in the temperature decrease as the flames are more uniform, subject largely to variations in scalar dissipation rate. Case 3 is somewhat more complicated. The RMS profiles begin low, then rise with flame extinction. The flames are nearly blown out and there is a period of mixing of combustion products with reactants during which the RMS temperature decreases. This profile then rises again during the reignition processes. The differences between the ODT and DNS RMS temperature profiles are directly attributable to the incomplete reignition achieved in the ODT cases. The fluctuations remain high since there are always significant regions of both burning and quenched flames at a given mixture fraction.

While the trend in the ODT RMS profiles is not correct, the shape and magnitude of the profiles are similar

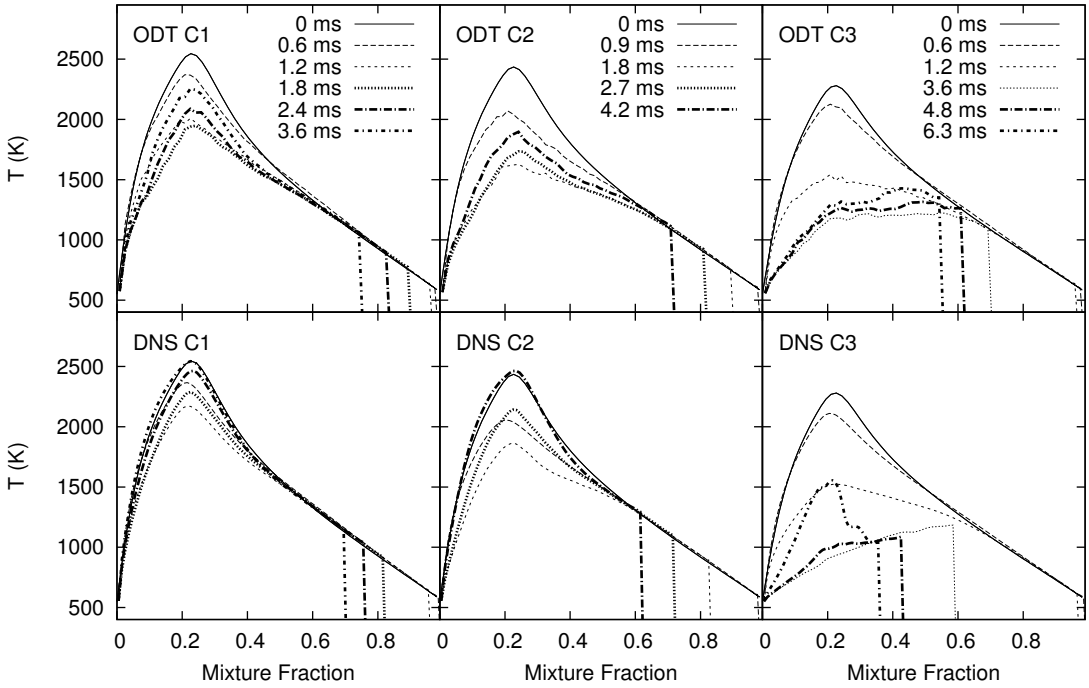


Figure 7: Conditional mean temperature profiles.

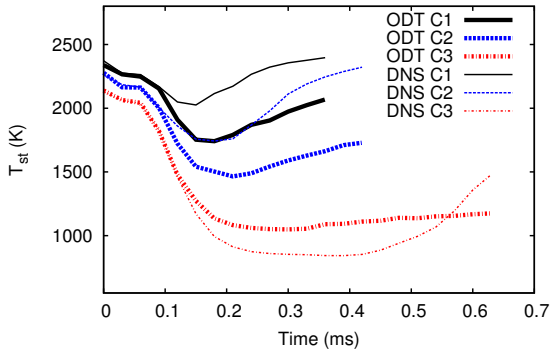


Figure 8: Stoichiometric mean temperatures as a function of time.

between the ODT and the DNS. For instance, the peak RMS temperature for Case 1 at 1.8 ms (near the time of peak extinction) is 600 K for the ODT and 400 K for the DNS. The RMS temperature at the same time for Case 2 is approximately 575 K for both the ODT and the DNS.

Like the temperature profiles, the mean DNS OH profiles initially decrease, then increase, while the ODT decrease, then increase, but do not fully recover. The conditional mean OH mass fraction profiles for Case 2 are shown in Fig. 10. The stoichiometric values at 1.8 ms are 0.0035, and 0.0055, for the ODT and DNS, respectively, consistent with the increased level of extinction of the DNS. The values for the ODT and DNS at 0.9 ms are very close.

Flame extinction and reignition is strongly influenced by the scalar dissipation rate. The stoichiometric mean and RMS fluctuations of the scalar dissipation rate $\chi_{st}$ are shown as functions of time for the three cases in Figs. 11 and 12. The shape and magnitude of the profiles are in very good agreement. For Cases 1 and 2, the mean $\chi_{st}$ peaks slightly later, and slightly higher than the corresponding DNS. This results in somewhat lower minimum temperatures, and minimum temperatures occurring later for Cases 1 and 2, as seen in Fig. 7. Similarly for these two cases, the value of the mean $\chi_{st}$ is higher in the reignition region past the peak for the ODT compared to the DNS. The increased peak dissipation rate is consistent with the increased level of flame extinction in the ODT for these cases. The mean $\chi_{st}$ is in very close agreement between the ODT and DNS for Case 3.

The ODT and DNS profiles of RMS $\chi_{st}$ are shown in Fig. 12. These profiles for a given case are similar in shape and magnitude. The profiles track closely in the early jet development (for $t < 0.1$ ms), after which the ODT attain a higher peak and slower decay than the DNS for Cases 1 and 2. The agreement between the ODT and DNS is very good for Case 3.

These higher RMS values for Cases 1 and 2, combined with the higher values of the mean $\chi_{st}$ at the peak and in the reignition region result in increased extinction, and exacerbate the weak ODT reignition processes. This occurs

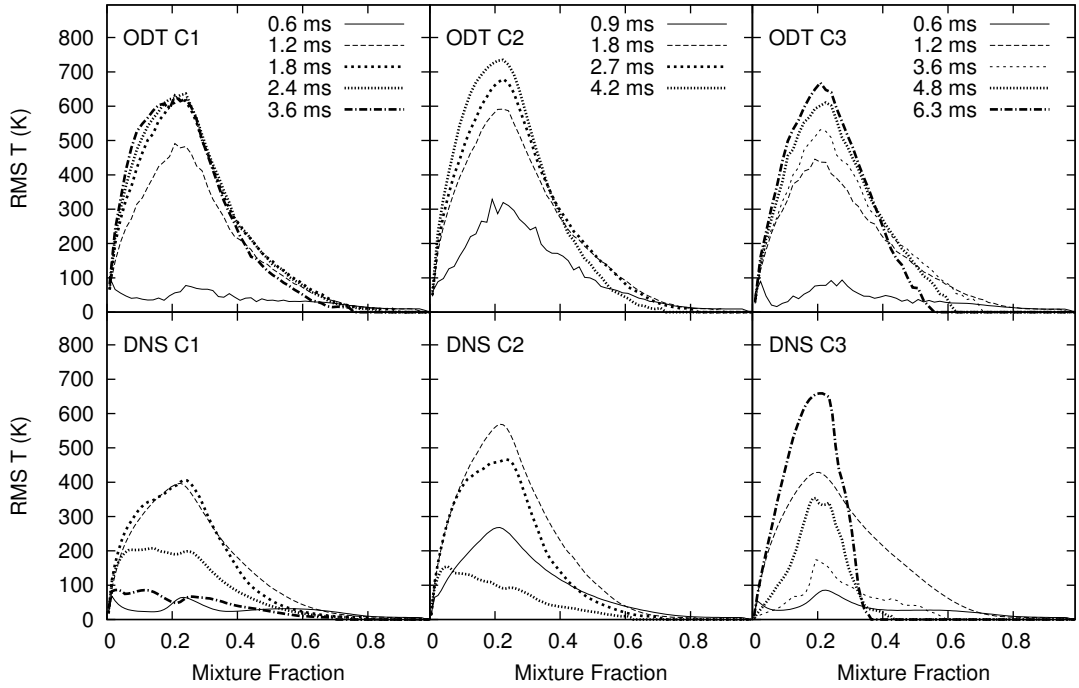


Figure 9: Conditional RMS temperature profiles.

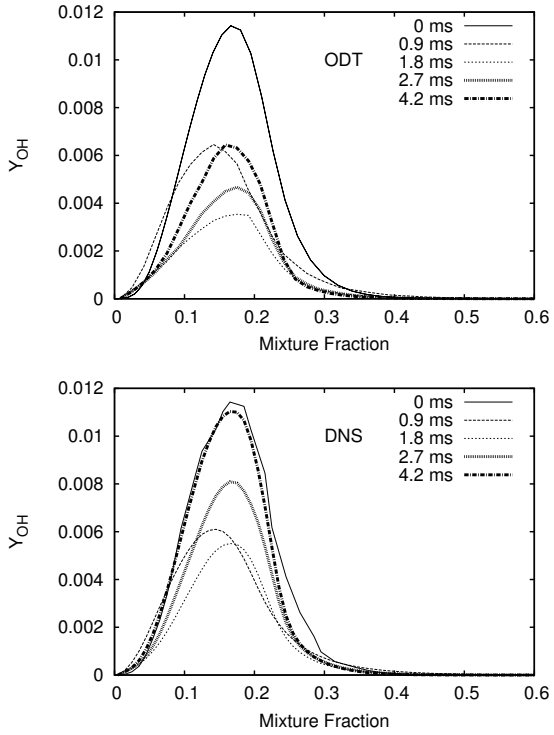


Figure 10: Conditional mean OH mass fraction profiles.

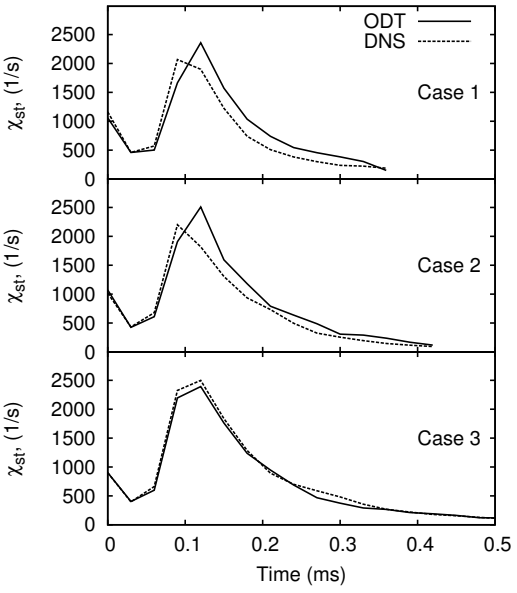


Figure 11: Stoichiometric mean scalar dissipation rate.

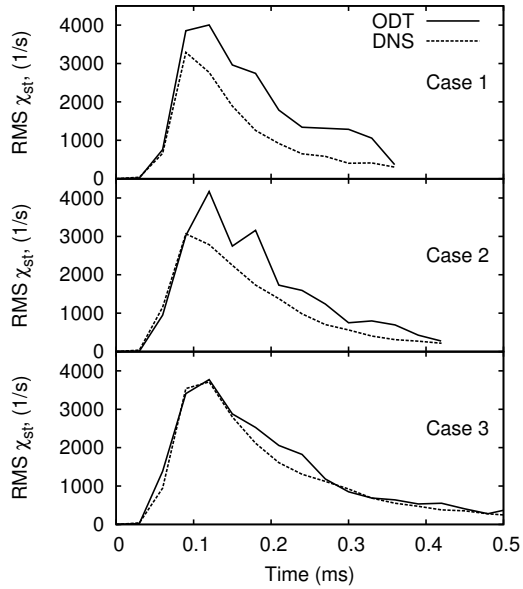


Figure 12: Stoichiometric RMS scalar dissipation rate.

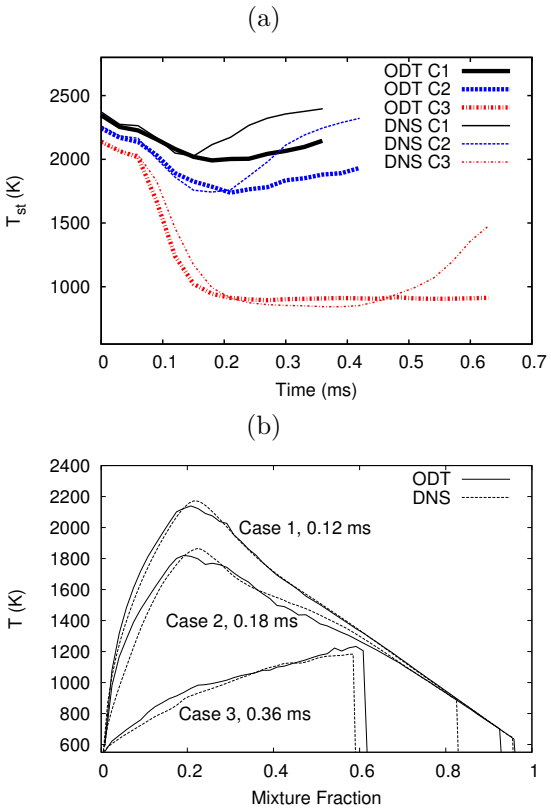


Figure 13: Stoichiometric mean temperature versus time (a); and conditional mean temperatures near times of peak extinction (b), both with retuned ODT parameters.

because higher mean and fluctuations of $\chi_{st}$ imply higher mixing rates at the flame surface. The heat release of reaction competes with the mixing rate, and when mixing rates exceed reaction rates flames tend toward extinction. Hence, the decreased flame reignition in ODT (compared to the DNS) is consistent with the higher mean and fluctuating stoichiometric scalar dissipation rates. However, the presence of flame tends to have a depressing effect on $\chi_{st}$ (through reduced mixing with flame dilatation) [26] so that it is not clear that the higher $\chi_{st}$ is a cause of the reduced reignition or a correlation. It is likely that the instantaneous nature of the triplet maps implemented for eddy events causes increased extinction in ODT. Extinction is a fast process dominated by the Kolmogorov-scale fluctuations [21], but still occurs over a finite time. The instantaneous triplet maps will increase the instantaneous dissipation rate felt by flames at the beginning of the diffusion process following an eddy event.

### *3.3. Retuned simulations*

While the ODT cases were performed with a single set of ODT parameters, results vary somewhat as the parameters change. Hewson and Kerstein [20] discussed the physical importance of the $C$ and $\beta$ parameters in turbulent $CO/H_2/N_2$ flames, and Gonzalez-Juez et al. [38] recently examined sensitivity to ODT parameters using the present ODT code in double-diffusive interfaces. Trends in Cases 1 and 2 do not change substantially with changes in the ODT parameters. However, Case 3 is near the global extinction limit, complicating comparison to the DNS. It is likely that reproduction of the DNS with a different random seed for the initial turbulence profile would result in blowout.

The ODT simulations presented above consist of a single set of parameters with values $C = 8$, $\beta = 0.8$ (and $Z = 400$). These values were determined primarily using the jet evolution and scalar dissipation statistics, with some consideration for the conditional mean temperature profiles. As shown, the results are generally good. The minimum ODT conditional mean temperatures are lower than the DNS by 200-300 K for Cases 1 and 2, and higher by approximately 300 K for Case 3 in the stoichiometric region. Somewhat better agreement is possible using different ODT parameters. Cases 1 and 2 were rerun with $C = 3$ and $\beta = 0.6$, and Case 3 was rerun with $C = 16$, $\beta = 0.8$. The conditional mean temperature near the time of peak flame extinction and the stoichiometric mean temperature as a function of time for these cases is shown in Fig. 13. Plot (a) of the figure can be compared directly to Fig. 8. The difference in the temperature profiles between the ODT and DNS in plot (b) is small. The difference among the curves for the three cases highlights the level of extinction between the three cases. The stoichiometric temperatures closely follow the DNS up to the point of reignition of the DNS.

Table 3: Stoichiometric mean temperatures at $t_1$=1.2, 1.8, and 3.6 ms (near peak extinction), and $t_2$=3.6, 4.2, and 6.3 ms (end time) for Cases 1, 2, and 3, respectively.

| | Simulation | T (K) at $t_1$ | T(K) at $t_2$ |
|---|---|---|---|
| Case 1 | DNS | 2048 | 2396 |
| | ODT $C = 3$, $\beta = 0.6$ | 2082 | 2145 |
| | ODT $C = 8$, $\beta = 0.8$ | 1910 | 2067 |
| Case 2 | DNS | 1744 | 2320 |
| | ODT $C = 3$, $\beta = 0.6$ | 1786 | 1932 |
| | ODT $C = 8$, $\beta = 0.8$ | 1504 | 1729 |
| Case 3 | DNS | 844 | 1475 |
| | ODT $C = 16$, $\beta = 0.8$ | 895 | 913 |
| | ODT $C = 8$, $\beta = 0.8$ | 1090 | 1174 |

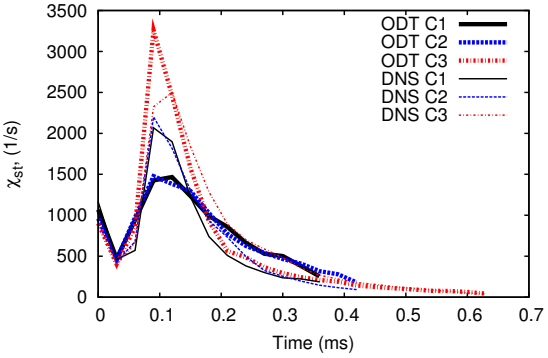


Figure 14: Stoichiometric scalar dissipation rates with retuned ODT parameters.

Table 3 compares the stoichiometric mean temperature at the times of peak extinction and at the end of the simulations. Results for the original and retuned ODT parameters are shown along with the DNS. The retuned Cases 1 and 2 have higher temperatures at peak extinction (Fig. 13), and higher temperatures at the end of the simulations. The reverse is true for Case 3.

The improved ODT/DNS agreement of the temperature profiles during extinction is paralleled by agreement of the conditional mean OH mass fraction profiles during the same period. For Case 2, the peak OH mass fraction, shown in Fig. 10, was 5% higher and 36% lower than the DNS at 0.9 and 1.8 ms, respectively. The retuned values are 15% and 4% higher at the same respective times. The time of 1.8 ms is approximately the time of peak extinction for Case 2, and 0.9 ms is intermediate.

The time evolution of the conditional mean $\chi_{st}$ is shown in Fig. 14. The shape and trend is similar between the ODT and DNS, but quantitative agreement of $\chi_{st}$ is sacrificed when attempting to capture the peak flame extinction. The ODT $\chi_{st}$ is lower than the DNS for Cases 1 and 2, and higher than the DNS for Case 3, consistent with the changes in the conditional temperature profiles for the retuned simulations. It is noted that scalar dissipation rate is a sensitive quantity, and in ODT a single triplet map increases local scalar dissipation by a factor of nine. The evolution of the mixture fraction (not shown) is very close to that reported in Fig. 5.

### *3.4. ODT parameter sensitivity*

The sensitivity of flame extinction and reignition to scalar dissipation rate and the flow evolution, and the demonstrated sensitivity of the ODT results to changes in the ODT parameters motivates investigation of the sensitivity of the present results to the ODT parameters. The physical importance of the ODT parameters has been discussed in the literature, e.g., [5, 16, 20]. Briefly, the $C$ parameter controls the overall eddy rate; the $\beta$ parameter controls the large eddy sizes, and hence affects the jet spread rate through entrainment of fluid into the jet; and the $Z$ parameter affects the small eddy suppression. See Eqs. (3-4).

Figure 15 shows the FWHM profiles, the stoichiometric temperature, and the stoichiometric scalar dissipation rate as a function of time for Case 2. Also shown is the eddy PDF for Case 2 integrated over the whole simulation. Three plots are shown, and within each, variation of $C$, $\beta$, and $Z$ are shown, along with the DNS for reference. The parameters are varied independently using the $C = 8$, $\beta = 0.8$, $Z = 400$ values as the baseline. Three values for each parameter are $C = 4$, 8, 16; $\beta = 0.4$, 0.8, 1.2; and $Z = 0$, 400, 800. (Six additional cases were run, each varying one of $C$ or $\beta$ or $Z$ from the baseline.) Each simulation (except the baseline used above) consists of 128 ODT realizations. The eddy PDFs shown are scaled by the average number of eddies per realization, which where 40, 56, and 73 for $C$ of 4, 8, and 16, respectively; 76, 56, and 41 for $\beta$ of 0.4, 0.8, and 1.2, respectively; and 747, 56, and 38 for $Z$ of 0, 400, and 800, respectively.

$C$ and $Z$ have minor effects on the FWHM profile but $\beta$ has a strong effect. This is directly related to the dependence of the large entraining eddies on $\beta$. Lower $\beta$ yields higher spread rates since, at a given time, lower $\beta$ allows higher eddy $\tau$ which is associated with larger eddies. The stoichiometric temperature is sensitive to all three parameters. While overall trends of extinction and reignition do not change with parameters, the quantitative results do. The mean flame (stoichiometric) temperatures shown are consistent with variation in the stoichiometric scalar dissipation rate. Higher $C$ and lower $\beta$ both yield higher $\chi_{st}$ and lower temperatures (higher extinction). The FWHM profile (jet width) increases with increasing $C$, but the effect is small here because the flame expansion from heat release is decreased by higher flame extinction as $C$ increases. Hence, as $C$ increases, there is a partial cancellation of the increasing width by increasing extinction. The sensitivity of results to $Z$ is fairly minor, and several earlier studies included a viscous penalty term, but not the $Z$ parameter [5, 16, 20, 21].

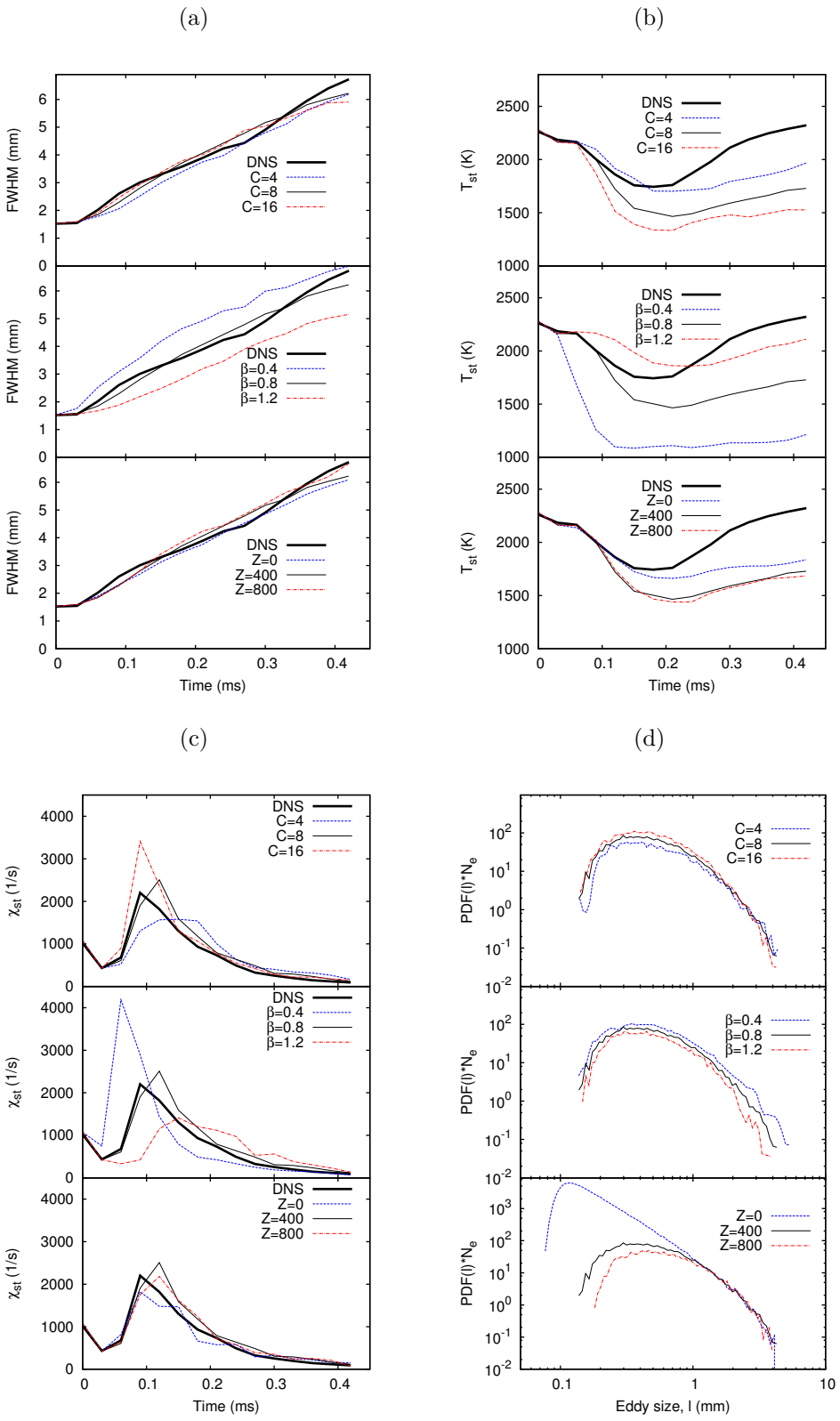


Figure 15: Sensitivity of FWHM profiles (a), $T_{st}(t)$ (b), $\chi_{st}(t)$ (c), and scaled eddy PDF (d) to changes in the $C$, $\beta$ and $Z$ ODT parameters.

The eddy PDFs show increasing numbers of eddies with increasing $C$. The allowance of larger eddies through smaller $\beta$ also increases the number of eddies. The shape of the unscaled PDFs (not shown) for $C$ changes are similar (likewise for $\beta$ changes), with somewhat higher probability of larger eddies with decreasing $\beta$ (noticeably) and $C$. The PDF for increasing $Z$ is shifted towards larger eddies since $Z$ penalizes small eddies. The $Z = 0$ curve shows the occurrence of many small eddies, but the number of larger eddies is the same as for the other two $Z$ values. This is consistent with the minor effect of $Z$ (of the smaller eddies) on the overall jet evolution (e.g., the FWHM plot) which is driven by the large eddies.

### *3.5. Reignition mechanism*

Under conditions of the present flames, the most likely reignition mechanisms will be flame propagation in a nonpremixed mode by flame folding (also called flame-flame interaction or FFI) or edge flames, or by premixed flame propagation in a premixed mode. Cases 1 and 2 were previously shown to reignite primarily through a nonpremixed mode, while Case 3 reignites through a premixed flame propagation mechanism [26]. Case 3 experiences extreme extinction followed by a long period in which products and reactants mix, followed by reignition via a premixed flame through a stratified mixture. For DNS Cases 1 and 2, visual evidence from animations of two-dimensional temperature profiles and three-dimensional renderings of the stoichiometric surface indicated significant reignition by edge flame propagation. Reignition by flame folding was also observed. The degree of each mode, however, has not yet been quantified.

ODT is able to capture reignition via premixed flame propagation and flame folding, but not edge flame propagation. Edge flames are inherently multi-dimensional with flames propagating along a nominally stoichiometric surface from a burning region to a quenched region [39]. As ODT represents a notional line of sight through a flow, the nearest it can come to representing flame propagation along an isosurface of mixture fraction is when the mixture fraction is uniform over a portion of the line. Even then, no transport orthogonal to the ODT domain direction is possible (or must be somehow modeled). Under these conditions, propagation via a premixed flame is possible, and may occur through a flammable stratified mixture. Flame folding occurs when two nominally stoichiometric mixtures, one burning and one quenched, are brought into proximity, and the burning region ignites the quenched region through diffusion of heat and mass.

In considering reignition in ODT via flame folding (that is, a burning stoichiometric region reigniting a nonburning one) it is interesting to compare the stoichiometric surface area in the ODT and the DNS. In DNS, the stoichiometric area is extracted directly using a marching cubes algorithm. In ODT, there is no real surface area, per se, but this quantity is approximated as the number of stoichiometric surface crossings times the x-z planar area (area normal to the line corresponding to the DNS). The number of stoichiometric crossings in the ODT is the number of crossings of the stoichiometric mixture fraction by the curve of mixture fraction versus position for a given ODT realization. The ODT and DNS surface area profiles coincide initially. Figure 16 compares the mean surface area of the DNS with the ODT ($C = 8$, $\beta = 0.8$ cases) as a function of time for the three cases. The ODT areas are shown as bold lines and the DNS as thin lines with Cases 1, 2, and 3, as solid, dashed, and dash-dot, respectively. The agreement between the ODT and DNS is quite remarkable, especially during the period of jet development and flame extinction. The agreement is very good for Case 2 throughout. The ODT overpredicts the DNS value for Case 1, and significantly underpredicts the value for Case 3. This lower area for ODT Case 3 is consistent with a decrease in stoichiometric surface area with decreased extinction (which the ODT underpredicts) since the heat release reduces local mixing [26]. However, note that the ODT results, while showing this same trend of increasing area with increasing degree of flame extinction, show much less variation among the three cases than the DNS.

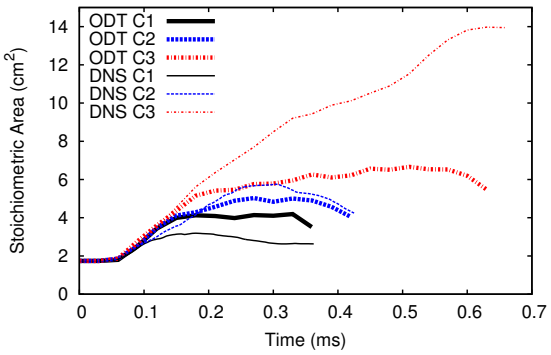


Figure 16: Stoichiometric surface area as a function of time for the three cases for ODT and DNS.

One should not compare ODT and DNS too literally here because of the different configurations and the ODT advective process. For instance, flame area in the DNS can increase without any apparent increase in the area as measured by a stoichiometric crossing on a line of sight in the y-direction times the x-z planar area. For example, initially planar flames wrinkled into a sine wave would have increased area, but as measured in ODT there would be no increase since the number of stoichiometric crossings along the corresponding line of sight would not increase. All transport in ODT occurs in the y-direction (direction of mean strain), whereas much of the DNS flame reignition occurs in the x-z direction.

The simulations investigated experience a very high degree of flame extinction. The DNS exhibit large regions that are quenched followed by flame reignition, especially for Cases 2 and 3. Considering Case 3, only a

small flame kernel survived extinction in the DNS and went on to relight the domain. Because the ODT domain is one-dimensional, the effective size of the domain is much smaller than that of the DNS. Whereas a small flame kernel can relight the whole DNS domain, the majority of the ODT realizations blow out. Loosely, suppose the probability of extinction in a given region were 99%, and the DNS domain were effectively 100 times that of the ODT (because of the extent of the domain in the periodic directions). Then, we would expect 1 out of 100 ODT realizations to relight, but the 1% of the DNS domain that is burning could relight the whole domain. Averaged over realizations, the ODT would register little reignition, while the DNS would register complete reignition. This problem motivates the development of three-dimensional grids of ODT lines for combustion problems, which would allow communication between lines. The proposed autonomous microstructure evolution (AME) model [40], and ODTLES models [14, 41, 15] are promising.

ODT realizations that blow out are determined by the peak temperature at the end of the simulation. A temperature of 1200 K is used as the criterion. The autoignition delay time of stoichiometric mixtures increases quickly below this temperature. Also, for Case 3, the peak temperatures at 6.3 ms for the realizations are bimodal with 96% of realizations either above 2200 K, or below 1200 K (for the $C = 16$, $\beta = 0.8$) case. For Cases 1 and 2 with $C = 3$, $\beta = 0.6$, that exhibited good temperature agreement at extinction, none of the realizations had peak end-time temperatures below 1200 K. Case 3 had 9 of 512 realizations below 1800 K. Hence, for Cases 1 and 2, blowout of realizations is not sufficient to account for the incomplete reignition. For Case 3, with $C = 16$ and $\beta = 0.8$, 78% of all realizations had peak end-time temperature below 1200 K, and 80% below 1800 K. This case showed little reignition from the low temperature. If we condition on burning realizations, the stoichiometric mean temperature at 0.36 ms is higher than the unconditional temperature: 1230 K versus 908 K, respectively. However, the corresponding conditional (on burning) temperature at 0.63 ms (the end of the simulation) is only 1318 K, 88 K higher.

The DNS Case 3 showed prominent reignition as a premixed flame [26]. This was analyzed by comparing the speed of the $Y_{\mathrm{CO2}} = 0.035$ isocontour (which correlated with heat release) to the corresponding local laminar premixed flame speed based on unburnt composition and temperature. During reignition, the average isocontour speed was very close to the average local laminar flame speed. The same analysis was repeated for ODT Case 3, considering all realizations and conditioning on burning realizations. Only fortuitous agreement of the isocontour speed with the laminar flame speed was observed, and there was no significant correlation, indicating little, if any, premixed flame propagation. This is not surprising given the low level of flame reignition. But, as noted, comparison of ODT with DNS for Case 3 is tenuous because of the level of extinction occurring.

## 4. Discussion

As noted in the introduction, Punati et al. [27] have recently performed a similar study comparing ODT to DNS with the same flow and geometrical configuration, but using a syngas fuel consisting of 50% CO (by volume), 10% $H_2$, and 40% $N_2$, giving a stoichiometric mixture fraction of 0.42 (with 75% $N_2$ and 25% $O_2$ in the oxidizer). The present ethylene flames are an ethylene/nitrogen mixture giving a stoichiometric mixture fraction $\xi_{st}$ of 0.17 [26]. In addition, Hewson studied syngas flames with 40% CO, 30% $H_2$, and 30%$N_2$ in air with a stoichiometric mixture fraction of 0.3 [20, 21].

Ethylene and syngas are significantly different fuels. Hewson and Kerstein [21] note the broad reaction zone thickness of syngas in the mixture fraction coordinate due to the high $\xi_{st}$ and the lack of strong fuel radical termination reactions in syngas compared to hydrocarbon combustion. Figure 17a shows heat release rates for steady laminar flamelet [42] solutions with unity Le at the extinction scalar dissipation rate $\chi_q$ for the three ethylene cases studied along with the syngas studied by Punati (from Hawkes et al. [28]). Also shown is an ethylene/nitrogen mixture with the same $\xi_{st}$, density ratio of reactants to products, flame kinematic viscosity, extinction scalar dissipation rate, and adiabatic flame temperature (remarkable) as the syngas (see [26]). The mixture fraction widths of the reaction zone as measured by the width of the profile at one-tenth the peak heat release rate are 0.30, 0.29, 0.28, 0.43, and 0.73 for Case 1, Case 2, Case 3, ethylene with $\xi_{st} = 0.42$, and syngas, respectively. The width of the syngas heat release rate profile is significantly greater than the ethylene cases, more than twice the present cases studied.

Also shown in Fig. 17b is the stoichiometric flamelet temperature as a function of the stoichiometric scalar dissipation rate. The extinction dissipation rate increases for the three ethylene cases studied here (4774, 3587, and 2380 for Cases 1, 2, and 3, respectively). The key result of the figure is the low extinction temperature of 1296 K for syngas compared to 1953, 1896, and 1822 for the ethylene cases (1, 2, 3, respectively), a difference of 526-657 K. The differences in the adiabatic flame temperatures are 193-345 K (Case 1 at the high end).

The wider reaction zone thickness and low extinction temperature of syngas compared to ethylene result in syngas having much stronger reignition characteristics than ethylene. The present ODT simulations contrast with those of Hewson and Punati in that the simulations of Hewson and Punati achieved strong (complete) reignition, whereas only partial flame reignition is observed here. Punati's ODT simulation showed higher flame extinction than the DNS, which occurred earlier than the DNS extinction. The reignition slightly exceeded that of the DNS. Punati's results are consistent with their stoichiometric scalar dissipation rate with a somewhat higher peak and occurring earlier than the DNS. The decay in the stoichiometric scalar

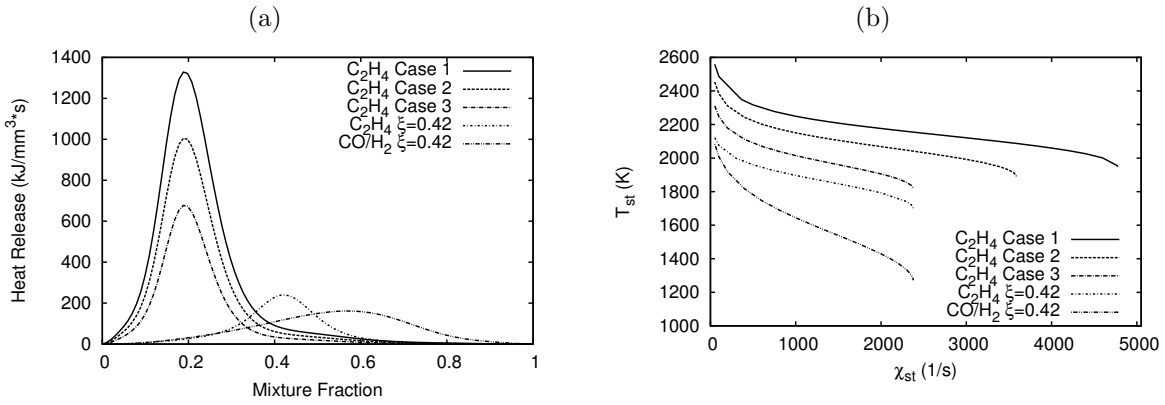


Figure 17: Flamelet heat release rate profiles for several cases (a); and stoichiometric flamelet temperatures as a function of stoichiometric scalar dissipation rate (b).

dissipation rate was faster after the peak than the DNS, and was lower by a factor of ∼3 around the time of reignition. (Punati et al. concede that optimization of model parameters may improve their results.) This low dissipation rate may account for the good reignition, but Hewson's flames also achieved good reignition and compared well with experiments [20].

Hewson described the key reignition mechanism in ODT as flame-flame interactions (FFIs) in which a burning stoichiometric zone reignites a nonburning one [20, 21]. He argues that FFI requires diffusional mixing out of nonflammable gas that separate the flame zones (burning or quenched) and that the wide reaction zone of syngas aids this processes. Here, we have demonstrated the wide reaction zone of syngas. As the reaction thickness decreases, such as for hydrocarbon combustion at lower $\xi_{st}$ studied here, a flamelet regime is approached. To quote Hewson and Kerstein [21, page 63]: "As one moves closer to the true flamelet regime, FFI becomes less likely because nonflammable regions are more likely to exist between flammable regions." Furthermore, the low extinction temperature of syngas results in relatively fewer fully quenched stoichiometric zones. In Hewson's flames, the width of the reaction zone is greater than the RMS mixture fraction fluctuations so that the flames were in a distributed reaction zone regime. However, the ratio of the reaction zone thickness to the RMS mixture fraction fluctuations for the present ethylene flames is 1.5 or greater.

To summarize, the increased difficulty for reignition by FFI for ethylene over syngas and the inability of ODT to capture reignition by edge flames results in the reduced reignition compared to the DNS. Quantification of the degree of reignition by edge flames and FFI is important, especially with changes in the Reynolds number. The present flames are at a moderate Reynolds number of 5120. Higher Reynolds number may shift the reignition mode towards FFI, which is discussed by Hewson and Kerstein [21].

The instantaneous nature of ODT triplet maps which increase local $\chi$ by a factor of nine (noted above) may also play a role, especially considering that extinction is a fast process compared to reignition [26, 21]. It may be possible to relax the high strain imposed by instantaneous triplet maps by modifying either their implementation, or by adjusting the diffusion process after an eddy event.

## 5. Conclusions

One-dimensional-turbulence simulations have been performed of flame extinction and reignition in nonpremixed, planar, temporally evolving ethylene jet flames. A series of three simulations were performed at constant Reynolds number, but decreasing Damköhler number, resulting in increasing levels of flame extinction. The ODT results were compared to direct numerical simulations of the same cases. The simulations were performed using the same thermodynamic, transport, and kinetic models in a compatible configuration. This correspondence allowed for a validation study of ODT by quantifying the level of agreement between the ODT and the DNS.

While ODT is a one-dimensional model in which advection is modeled through stochastic eddy events, the resolution of fine-scale reactive and diffusive structures is an advantage of the model. The computational cost is orders of magnitude lower than a corresponding DNS simulation, which allows ODT simulations to be run under conditions not available to DNS (such as high Reynolds number), or allows many more parametric studies to be performed. As such, quantifying the limitations of ODT is important.

The ODT presented here were able to capture the evolution of the jet, as well as heat release effects. The prediction of the scalar dissipation statistics by ODT is quite good, especially for the baseline simulations. However, the corresponding level of extinction for Cases 1 and 2 was overpredicted. Retuned parameters gave very good agreement with DNS for conditional mean temperatures at extinction, but less quantitative agreement for scalar dissipation rate. However, scalar dissipation rate is very challeng-

ing to model in reacting flows. Sensitivity to model parameters was performed to illustrate parameter effects on the flow evolution, scalar dissipation rate, and flame extinction and reignition. The large eddy suppression parameter $\beta$ and the eddy rate parameter $C$ had the strongest effect on the flow, but no significant qualitative changes in the jets were observed.

While the ODT was able to capture the flame extinction processes, the reignition process was less well represented, in contrast to previous ODT simulations using syngas fuel. This is due to the smaller reaction zone thickness and higher extinction temperature of ethylene compared to syngas, and the inability of ODT to capture three-dimensional flame structures such as edge flames, which appear to be an important reignition mechanism in the DNS. ODT is able to capture reignition processes through flame folding, and some degree of reignition was observed in all the ODT simulations. The rate of reignition by edge flames is diffusively controlled, but the rate of reignition by flame folding is controlled by advection, so the spread of reignition over large distances should be dominated by an advective rather than diffusive mechanism, hence by flame folding. Therefore, the ODT representation of reignition should improve with increasing Reynolds number and consequent increase of the range of advective scales. Running DNS cases such as those considered here for a range of Reynolds numbers might give an indication of the validity of this conjecture.

The comparison of the ODT to the DNS was somewhat better for Cases 1 and 2 than for Case 3. Case 3 exhibits near blowout conditions, and reignites as a premixed flame. Consequently, this case is difficult to capture in ODT (and would be difficult to reproduce in DNS).

Given the level of fine-scale fidelity built into ODT through accurate chemical and transport models, and good flow modeling, and given the difficulty of capturing the reignition process, it is evident that other more reduced combustion models will be challenged to capture flame extinction and reignition processes.

## 6. Acknowledgment

The authors thank Alan Kerstein for helpful insights and discussions, as well as his encouragement and enthusiasm for this work.

## References

[1] J. H. Chen, A. Choudhary, B. de Supinski, M. DeVries, E. R. Hawkes, S. Klasky, W. K. Liao, K. L. Ma, J. Mellor-Crummey, N. Podhorszki, R. Sankaran, S. Shende, C. S. Yoo, Computational Science and Discovery 2 (2009) 1–31.
[2] A. R. Kerstein, Journal of Fluid Mechanics 392 (1999) 277–334.
[3] A. R. Kerstein, W. T. Ashurst, S. Wunsch, V. Nilsen, Journal of Fluid Mechanics 447 (2001) 85–109.
[4] W. T. Ashurst, A. R. Kerstein, Physics of Fluids 17-025107 (2005) 1–26.
[5] A. R. Kerstein, T. D. Dreeben, Physics of Fluids 12 (2000) 418–424.
[6] T. D. Dreeben, A. R. Kerstein, International Journal of Heat and Mass Transfer 43 (2000) 3823–3834.
[7] H. Shihn, P. E. DesJardin, International Journal of Heat and Mass Transfer 50 (2007) 1314–1327.
[8] W. T. Ashurst, A. R. Kerstein, L. M. Pickett, J. B. Ghandhi, Physics of Fluids 15 (2003) 579–582.
[9] S. Wunsch, A. R. Kerstein, Journal of Fluid Mechanics 528 (2005) 173–205.
[10] S. Wunsch, A. Kerstein, Physics of Fluids 13 (2001) 702–712.
[11] A. R. Kerstein, R. C. Schmidt, S. Wunsch, W. T. Ashurst, V. Nilsen, T. D. Dreeben, High-resolution modeling of multiscale transient phenomena in turbulent boundary layers, SAND2001-8108, Technical Report, Sandia National Laboratories, Livermore, CA, 2001.
[12] R. C. Schmidt, A. R. Kerstein, S. Wunsch, V. Nilsen, Journal of Computational Physics 186 (2003) 317–355.
[13] A. R. Kerstein, Computer Physics Communications 148 (2002) 1–16.
[14] R. Schmidt, R. McDermott, A. Kerstein, ODTLES: A model for 3D turbulent flow based on one-dimensional turbulence modeling concepts, SAND2005-0206, Technical Report, Sandia National Laboratories, Livermore, CA, 2005.
[15] S. Cao, T. Echekki, Journal of Turbulence 9 (2008) 1–35.
[16] T. Echekki, A. R. Kerstein, T. D. Dreeben, Combustion and Flame 125 (2001) 1083–1105.
[17] B. Ranganath, T. Echekki, Progress in Computational Fluid Dynamics 6 (2006) 409–418.
[18] B. Ranganath, T. Echekki, Combustion and Flame 154 (2008) 23–46.
[19] H. Shihn, P. E. DesJardin, in: Proceedings of IMECE04 ASME International Mechanical Engineering Congress and Exposition, 2004, Anaheim, CA.
[20] J. C. Hewson, A. R. Kerstein, Combustion Theory and Modelling 5 (2001) 669–697.
[21] J. C. Hewson, A. R. Kerstein, Combustion Science and Technology 174 (2002) 35–66.
[22] A. J. Ricks, J. C. Hewson, A. R. Kerstein, J. P. Gore, S. R. Tieszen, W. T. Ashurst, Combustion Science and Technology 182 (2010) 60–101.
[23] J. C. Hewson, A. J. Ricks, S. R. Tieszen, A. R. Kerstein, R. Fox, in: Center for Turbulence Research, Proceedings of the Summer Program, 2006.
[24] J. Hewson, A. Ricks, S. Tieszen, A. Kerstein, R. Fox, in: H. Bockhorn, A. D'Anna, A. Sarofim, H. Wang (Eds.), Combustion Generated Fine Carbonaceous Particles, Karlsruhe University Press, Karlsrue Germany, 2009, pp. 571–587.
[25] D. O. Lignell, J. C. Hewson, J. H. Chen, Proceedings of the Combustion Institute 31 (2009) 1491–1498.
[26] D. O. Lignell, J. H. Chen, H. A. Schmutz, Combustion and Flame 158 (2011) 949–963.
[27] N. Punati, J. C. Sutherland, A. R. Kerstein, E. R. Hawkes, J. H. Chen, Proceedings of the Combustion Institute 33 (2011) 1515–1522.
[28] E. R. Hawkes, R. Sankaran, J. H. Chen, in: $5^{th}$ Joint US Combustion Meeting of the Combustion Institute, p. B05.
[29] R. J. McDermott, Toward one-dimensional turbulence subgrid closure for large-eddy simulation, Ph.D. thesis, The University of Utah, 2005. http://search.proquest.com/docview/305401834.
[30] P. A. Lewis, G. S. Shedler, Naval Res. Logistics Quart. 26 (1979) 403–413.
[31] A. Papoulis, S. U. Pillai, Probability, Random Variables, and Stochastic Processes, McGraw-Hill, New York, fourth edition, 2002.
[32] W. T. Ashurst, A. R. Kerstein, Physics of Fluids 21-119901 (2009) 1.
[33] D. O. Lignell, A. Kerstein, G. Sun, E. I. Monson, Mesh adaption for efficient multiscale implementation of one-dimensional turbulence, 2012. Theoretical and Computational Fluid Dynamics, in press.
[34] D. Goodwin, Cantera, an object-oriented software toolkit for

chemical kinetics, thermodynamics, and transport processes, 2011. http://code.google.com/p/cantera.
[35] D. O. Lignell, J. H. Chen, P. J. Smith, T. Lu, C. K. Law, Combustion and Flame 151 (2007) 2–28.
[36] J. D. Hoffman, Numerical Methods for Engineers and Scientists, CRC Press, New York, 2001.
[37] S. Cohen, A. Hindmarsh, Computers in Physics 10 (1996) 138–143. http://llnl.gov/casc/sundials/.
[38] E. Gonzalez-Juez, A. R. Kerstein, D. O. Lignell, Journal of Fluid Mechanics 677 (2011) 218–254.
[39] C. Pantano, Journal of Fluid Mechanics 514 (2004) 231–270.
[40] A. R. Kerstein, Lecture Notes in Physics 756 (2009) 291–333.
[41] R. C. Schmidt, A. R. Kerstein, R. McDermott, Comput. Methods Appl. Mech. Engrg. 199 (2010) 865–880.
[42] N. Peters, Progress in Energy and Combustion Science 10 (1984) 319–339.